

Received November 17, 2020, accepted December 7, 2020, date of publication December 25, 2020, date of current version January 4, 2021.

Digital Object Identifier 10.1109/ACCESS.2020.3046886

# Active Vibration Isolation of a Maglev Inertially Stabilized Platform Based on an Improved Linear Extended State Observer

WANFA SHI<sup>1</sup>, KUN LIU<sup>2</sup>, AND WENPENG ZHAO<sup>3</sup>, (Member, IEEE)

<sup>1</sup>Aerospace College, Sun Yat-sen University, Guangzhou 510006, China

<sup>2</sup>College of Aerospace Science and Engineering, National University of Defense Technology, Changsha 410073, China

<sup>3</sup>Sun Yat-Sen University, Guangzhou, Guangdong, China

Corresponding author: Kun Liu (liukun6@mail.sysu.edu.cn)

This work was supported in part by the Natural Science Foundation of Shenzhen, China, under Grant 2020N015.

**ABSTRACT** An inertially stabilized platform is subject to the vibration force and moment from its support base, and low-frequency vibrations cannot be eliminated by mechanical vibration isolation. Combining gimbals with magnetic bearings instead of mechanical bearings, a maglev inertially stabilized platform (MISP) is characterized by no friction or an active vibration control capability. In this paper, an improved linear extended state observer (LESO) replacing displacement error with next-order error is proposed to estimate the low-frequency vibration and improve the estimation accuracy. An active vibration isolation control method is then designed to realize cancellation compensation on the MISP. Finally, a simulation example is presented to validate that the proposed measures can effectively eliminate the low-frequency vibration force transmitted from the base and ensure the stability of the MISP.

**INDEX TERMS** Maglev inertially stabilized platform, low-frequency vibration, active vibration isolation technology, improved linear extended state observer.


## I. INTRODUCTION

A maglev inertially stabilized platform (MISP) is a new type of inertially stabilized platform (ISP) that utilizes magnetic bearings instead of mechanical bearings. Compared with traditional inertially stabilized platforms, a MISP is free of friction and provides excellent disturbance rejection. The MISP is able to isolate various disturbances from a carrier and provides better line of sight (LOS) stabilization for the high-precision positioning systems used in aviation remote sensing. In the late 1980s, a single-axis magnetic gimbal system was developed with a LOS accuracy from 3 to 8  $\mu$ rad under an angular disturbance of 48 rad/s [1], [2]. In recent years, the high performance of MISPs [3], [4] has garnered considerable attention.

The performance of a MISP can be restricted by factors such as a change in the platform load, a disturbance acting on the platform [5], and a vibration force and vibration moment from a pitching frame. The combination of magnetic suspension control [6] and inertial stabilized platform control [7] has been studied to reduce the impact of the

above disturbances. In [8], an adaptive control strategy was applied in an ISP and confirmed experimentally. A reduced-order disturbance observer [9] was relatively insensitive to the parameters of a gimble control system and was easy to implement in engineering. Fuzzy control has been adopted for the stability of ISP control systems, and research [10] has concentrated on improving the transient process and tracking accuracy of rotating shafts. Many efforts have been made to counter magnetic bearing control [11]–[17], which has a significant impact on the performance of MISPs. In [11], a PD controller and PID controller were adopted in a magnetic bearing control to obtain an ideal result. The  $H_\infty$  method [13] and a quantitative feedback principle [14] were employed in many studies due to the boundedness of linear models.

Input vibration is a common disturbance when actuators are employed. Passive vibration isolation [18], [19] is based on a spring-damper structure, which is suitable for high-frequency vibration isolation (>20 Hz) but is unable to suppress low-frequency vibrations (<20 Hz) effectively. Because of the characteristics of low-frequency vibration, active vibration isolation introduces feedback variables through the motion measurement of sensors and suppresses input vibration with a certain control strategy. A method [20]

The associate editor coordinating the review of this manuscript and approving it for publication was Luigi Biagiotti .

for structural optimization design and cascade PID control of maglev actuators was proposed based on the principle of the Lorentz force. The application of a cascade PID control method managed to attenuate the control object in a range of  $-22.522$  to  $-2.189$  dB within a 1–25 Hz band and perform effective vibration control. Alternatively, vibration signals can be treated as systematic external disturbances in the input channel. Vibration isolation can also be achieved by disturbance compensation. Observer technology has been widely investigated and applied in the area of disturbance rejection, including vibration isolation. A better observer can obtain a better estimation of disturbance, which is of great significance for improving control precision. Generally, the performance of an observer is evaluated by the observation accuracy and convergence rate. By combining observers, feedback and disturbance compensation can effectively suppress systematic disturbances such as saturation, friction torque, unmodeled nonlinearities and uncertainties. In [21], a novel fast nonsingular terminal slide model control scheme with an adaptive disturbance observer was developed for an active suspension system, and the system state could converge to arbitrarily small bounds within a finite time in the presence of estimation error. In [22], a novel disturbance observation-based robust control method was proposed that could be applied in practical active-passive vibration isolation systems, which obtained stable precision and outstanding transient performance. A new output feedback control method with an elaborately designed observer was proposed in [23], and it could precisely estimate the velocity and constrain the control inputs within the permitted ranges, which contributed to rapid jib and trolley positioning and payload sway suppression.

A control system for a MISP [3], [24] based on PID and dual-stage systems was structured that able to realize disturbance rejection to a certain extent but had difficulty suppressing vibrations at low frequencies. There is little research on active vibration isolation control for this kind of actuator. Therefore, it is meaningful and necessary to study effectively isolating the low-frequency vibrations from the base to improve the performance of the MISP and provide smooth working conditions for payloads. In this paper, we address the suppression effect for low-frequency vibrations on a MISP. An improved linear extended state observer [25]–[28] is designed to estimate the dynamic input vibration, which uses next-order error to substitute the first-order error (displacement error) to speed up the convergence, and the observation error is reduced significantly, which is theoretically deduced and proven. In addition, a vibration isolation controller is built to compensate for the input vibration and eliminate the adverse effects of input vibration.

This paper is structured as follows. The decoupling control model of MISP is described in Section II. In Section III, an improved linear extended state observer for the MISP model is built for disturbance estimation with higher accuracy. Then, a vibration isolation controller is designed based on the previous control model. A simulation example is

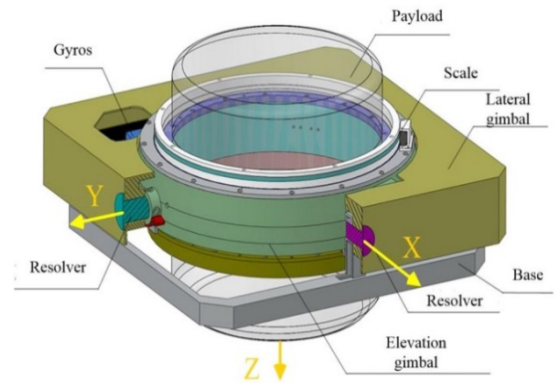


FIGURE 1. The MISP structure.

provided to verify the arguments in Section IV. A conclusion is drawn in Section V.

## II. THE MISP CONTROL MODEL

### A. BASIC STRUCTURE

A structural diagram of the MISP is shown in Fig. 1. The frame of the MISP is composed of a base assembly, a lateral outside gimbal, and an elevated inner gimbal. The base assembly is installed on the vehicle via four shock absorbers to eliminate high-frequency vibrations from the vehicle. The lateral gimbal is connected to the base through mechanical bearings and rotates around the longitudinal axis of the vehicle. The elevation gimbal is also combined with the lateral gimbal through mechanical bearings in the perpendicular direction in the horizontal plane. It utilizes motor–gear systems to drive the gimbals. Resolvers are mounted on the end of the axes to measure the gimbal angles, which are restricted in a sway of  $\pm 8^\circ$ . Angular rate gyros are installed on the elevation gimbal in the corresponding directions to furnish angular velocity feedback for the stabilizing loops in both directions. The payload instrument is suspended by gimbals, which forms the magnetic levitation system. Platform controllers are installed on the corners of the lateral gimbal. The motion and force diagram of the MISP is depicted in Fig. 2. The payload instrument is magnetically levitated in 5DOFs, including axial translation along Z, radial translation along X' and Y', and slight rotation around the axial X and axial Y. The forces at four locations are combined and simplified to  $F_A, F_B, F_C$  and  $F_D$  for analyzing the kinetic model with

$$F_A = f_{Au} - f_{Ad}, \quad F_B = f_{Bu} - f_{Bd}, \quad F_C = f_{Cu} - f_{Cd}, \\ F_D = f_{Du} - f_{Dd}$$

### B. SYSTEM MODEL

The theoretical magnetic force at the nominal position with linearization is given as:

$$F = k_i \Delta i + k_x \Delta x \tag{1}$$

where  $\Delta x$  is the displacement to the nominal position,  $\Delta i$  is the control current,  $k_i$  is the current stiffness, and  $k_x$  is the displacement stiffness. A dynamic model of the MISP under

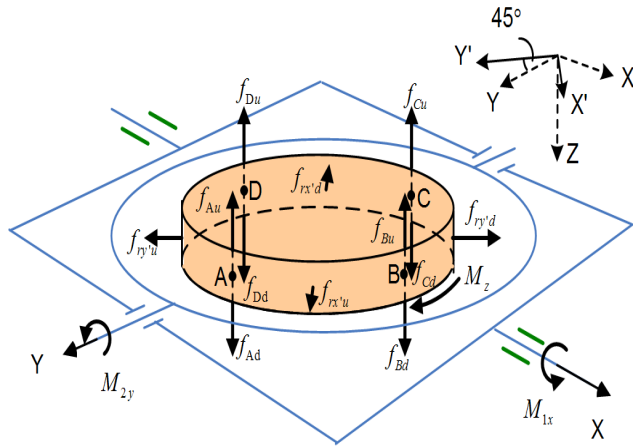


FIGURE 2. The MISP motion and force diagram.

the above conditions can be written as:

$$\begin{cases} mx_z = F_A + F_B + F_C + F_D \\ J_r \ddot{\varphi} = R(F_C - F_A) \\ J_r \ddot{\theta} = R(F_B - F_D) \end{cases} \quad (2)$$

which can also be rewritten as:

$$M \ddot{\mathbf{x}} = F_{kin} \mathbf{f} \quad (3)$$

$$M = \text{diag}(m \ J_r \ J_r) \quad (4)$$

$$F_{kin} = \begin{bmatrix} 1 & 1 & 1 & 1 \\ -R & 0 & R & 0 \\ 0 & R & 0 & -R \end{bmatrix} \quad (5)$$

where  $m$  is the mass of the platform,  $J_r$  is the radial inertia, and  $R$  represents the radius of the platform.  $x_z$ ,  $\varphi$ , and  $\theta$  are the displacement in the  $Z$  axis direction and the radial rotation around the  $X$  and  $Y$  axes, respectively.  $F_A$ ,  $F_B$ ,  $F_C$ , and  $F_D$  are the forces on four positions.  $\mathbf{x}$  is the position vector of the levitated platform, given as  $\mathbf{x} = (x_z \ \varphi \ \theta)'$ , and  $\mathbf{f}$  is the force vector, given as  $\mathbf{f} = (F_A \ F_B \ F_C \ F_D)'$ .

As (2) shows, axial translation control and radial rotation control are implemented by the four-point position electromagnetic force, and the two control channels have a coupling relation. The displacement sensors are installed at the same position on which the control force works, and the displacements measured by the sensor satisfy the coupling relation because they are in the same plane, given as:

$$s_A + s_C = s_B + s_D \quad (6)$$

where  $s_A$ ,  $s_B$ ,  $s_C$ , and  $s_D$  are the measured displacements by sensors, written as  $\mathbf{s} = (s_A \ s_B \ s_C \ s_D)'$ . The relation between  $\mathbf{s}$  and  $\mathbf{x}$  can be deduced as:

$$\mathbf{s} = T_{tran} \mathbf{x} \quad (7)$$

$$T_{tran} = \begin{bmatrix} 1 & -R & 0 \\ 1 & 0 & R \\ 1 & R & 0 \\ 1 & 0 & -R \end{bmatrix} \quad (8)$$

(7) and (8) show that the absolute displacement of the stable platform corresponds to the axial displacement of the four

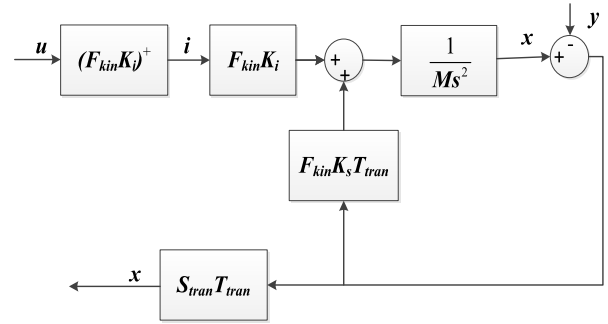


FIGURE 3. Decoupling control system diagram of MISP.

points (A, B, C, and D). The control current of the four points is recorded as  $\mathbf{i} = [i_A \ i_B \ i_C \ i_D]'$ . The electromagnetic force can be expressed as:

$$\mathbf{f} = \mathbf{K}_i \mathbf{i} + \mathbf{K}_s \mathbf{s} \quad (9)$$

$$\mathbf{K}_i = \text{diag}(k_{ai} \ k_{ai} \ k_{ai} \ k_{ai}) \quad (10)$$

$$\mathbf{K}_s = \text{diag}(k_{as} \ k_{as} \ k_{as} \ k_{as}) \quad (11)$$

where  $k_{ai}$  is the current stiffness coefficient of a single axial electromagnet and  $k_{as}$  is the displacement stiffness coefficient of a single electromagnet. From (5), (7), and (11), the equivalent displacement stiffness matrix of the stable platform in three degrees of freedom of axial translation and radial rotation can be deduced as:

$$\mathbf{K}_x = F_{kin} \mathbf{K}_s T_{tran} = \begin{bmatrix} 4k_{as} & & \\ & 2k_{as}R^2 & \\ & & 2k_{as}R^2 \end{bmatrix} \quad (12)$$

where  $\mathbf{K}_x$  is the equivalent displacement stiffness matrix, which realizes the decoupled control between 3DOFs (an axial movement and two radial rotations). Each control channel is controlled independently. Thus, (3) can be written as:

$$M \ddot{\mathbf{x}} = \mathbf{u} + \mathbf{k}_x \mathbf{x} \quad (13)$$

where  $\mathbf{u}$  is taken as the control input and written as  $\mathbf{u} = (u_z \ u_\varphi \ u_\theta)'$ . The relation between  $\mathbf{i}$  and  $\mathbf{u}$  can be obtained as:

$$\mathbf{i} = (F_{kin} \mathbf{K}_i)^+ \mathbf{u} \quad (14)$$

where  $(F_{kin} \mathbf{K}_i)^+$  indicates the Moore inverse matrix of  $(F_{kin} \mathbf{K}_i)$ .

A control block diagram of the MISP is shown in Fig. 3, where  $S_{tran}$  is given as:

$$S_{tran} = \begin{bmatrix} \frac{1}{4} & \frac{1}{4} & \frac{1}{4} & \frac{1}{4} \\ -\frac{1}{2R} & 0 & -\frac{1}{2R} & 0 \\ 0 & -\frac{1}{2R} & 0 & -\frac{1}{2R} \end{bmatrix} \quad (15)$$

### III. ACTIVE VIBRATION ISOLATION CONTROL

#### A. EXISTING VIBRATION ISOLATION EFFECT

During the flight of the aircraft, there will be some vibration on the base surface of the MISP. Without corresponding measures, the vibration will be transmitted to the platform

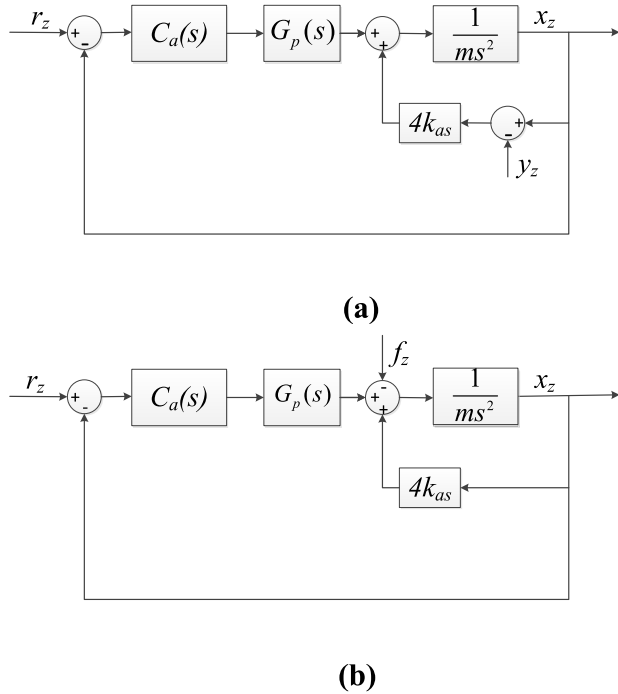


FIGURE 4. (a) Control diagram of input vibration displacement (b) Control diagram of the input vibration force with equivalent conversion.

through the pitch frame, causing a change in the air gap of the electromagnet, and the platform will be affected by the negative displacement stiffness and gradually destabilize and deviate from the equilibrium position. Generally, spring-damped oscillators are used to isolate vibrations greater than 20 Hz in engineering but are unable to eliminate vibrations lower than 20 Hz. This section introduces a method that combines an improved extended state observer with an active vibration isolation controller to eliminate the low-frequency vibration effectively.

In view of the decoupling of the axial displacement control and the radial rotation control achieved in the previous chapter, the analysis and design of the vibration isolation controller \$G\_{ia}(s)\$ are performed through the axial displacement control structure. The corresponding vibration isolation controller for radial rotation can be obtained by an identical method.

The block diagram of axial displacement control is depicted in Fig. 4(a), where \$y\_z\$ represents the input vibration displacement from the pitch frame and \$G\_p(s)\$ represents the power amplification. The input vibration force is depicted as in Fig. 4(b).

As Fig. 4 shows, \$C\_a(s)\$ is the axial displacement anti-disturbance controller, which adopts a PID controller in series connection with a first-order filter \$G\_p(s)\$ to suppress the high-frequency noise, given as:

$$C_a(s) = \frac{1}{\tau_f s + 1} \left( K_p + \frac{K_d s}{0.0001s + 1} + \frac{K_I}{s} \right) \quad (16)$$

$$G_p(s) = \frac{1}{\tau_{mag} s + 1} \quad (17)$$

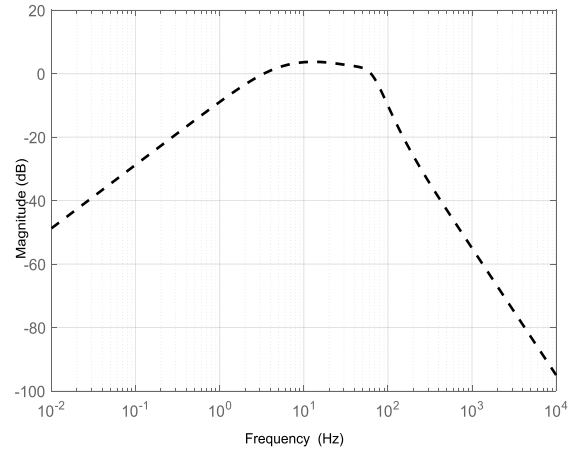


FIGURE 5. Frequency response of the transfer function.

where \$\tau\_f\$ is the filter coefficient and \$K\_p K\_d\$, and \$K\_I\$ represent the proportional, differential, and integral coefficients, respectively. \$r\_z\$ represents the reference values of the working point at the equilibrium position, generally taken as zero, and \$x\_z\$ represents the axial output displacement.

As a result, we can obtain the vibration transfer functions from \$f\_z\$ to \$x\_z\$ as follows:

$$G_z(s) = \frac{X_z(s)}{F_z(s)} = \frac{-1}{ms^2 + C_a(s)G_p(s) - 4k_{as}} \quad (18)$$

The frequency response is depicted in Fig. 5.

As depicted in Fig. 5, the magnitude in most frequency bands of 1-100 Hz is approximately 0 dB, which means that there is no effective improvement in vibration isolation. This suggests that the existing maglev control system is unable to eliminate the input vibration, and other measures are thus necessary.

### B. IMPROVED LINEAR EXTENDED STATE OBSERVER

AS presented by Han [27], the extended state observer (ESO) is a prominent part of ADRC technology that is able to effectively estimate the disturbance acting on a system. A linear extended state observer (LESO) [26] is a form of improved ESO and is used to adjust parameters in engineering applications.

For a SISO 2nd-order system:

$$\begin{cases} \ddot{x} = f(x, \dot{x}, p(t)) + bu(t) \\ y = x \end{cases} \quad (19)$$

where \$x\$, \$\dot{x}\$, and \$\ddot{x}\$ are the state variables, \$u(t)\$ is the measured output, and the parameter \$b\$ is the control gain. Let \$x\_1 = x\$, \$x\_2 = \dot{x}\$, and \$x\_3 = \ddot{x} - bu\$, where \$x\_3\$ is an extended state regarded as the total disturbance; the extended state-space equation after extension is given as:

$$\begin{cases} \dot{x}_1 = x_2 \\ \dot{x}_2 = x_3 + bu \\ \dot{x}_3 = d(t) \\ y = x_1 \end{cases} \quad (20)$$

where  $d(t)$  represents the derivative of the total disturbance. From (19), we can establish the 3rd-order LESO:

$$\begin{cases} e = z_1 - x_1 \\ \dot{z}_1 = z_2 - \beta_1 e \\ \dot{z}_2 = z_3 - \beta_2 e + bu \\ \dot{z}_3 = -\beta_3 e \end{cases} \quad (21)$$

Given that the displacement error  $e$  declines continuously, the gain coefficients  $\beta_1, \beta_2$  and  $\beta_3$  must be high enough to allow  $z_2$  and  $z_3$  to keep up with  $x_2$  and  $x_3$ , which will destroy the dynamic performance of the control system.

To accelerate the convergence rate and improve the error accuracy with suitable gain, this paper adopts a method based on the track error of each order to enhance the estimation accuracy of LESO [28], which can meet the accurate compensation requirements of the active vibration isolation control system of a MISP. The improved LESO is given as:

$$\begin{cases} e_1 = z_1 - x_1 \\ \dot{z}_1 = z_2 - \beta_1 e_1 \\ \dot{z}_2 = z_3 - \beta_2 e_2 + bu \\ \dot{z}_3 = -\beta_3 e_3 \end{cases} \quad (22)$$

where  $e_1, e_2$  and  $e_3$  represent the track errors of  $z_1$  and  $x_1, z_2$  and  $x_2$  and  $z_3$  and  $x_3$ . We define  $\mathbf{x}_a = [x_{a1} \ x_{a2} \ x_{a3}]'$ , where  $x_{a1}, x_{a2}$  and  $x_{a3}$  represent axial displacement, axial translation speed and acceleration, respectively. The governing equation of the MISP is given as:

$$\begin{cases} \dot{x}_{a1} = x_{a2} \\ \dot{x}_{a2} = x_{a3} + \frac{u}{m} + cx_{a1} \\ \dot{x}_{a3} = p(t) \end{cases} \quad (23)$$

The improved ESO model for the MISP can be constructed as:

$$\begin{cases} \dot{z}_{a1} = z_{a2} - \beta_1 e_{a1} \\ \dot{z}_{a2} = z_{a3} - \beta_2 e_{a2} + \frac{u}{m} + cz_{a1} \\ \dot{z}_{a3} = -\beta_3 e_{a3} \end{cases} \quad (24)$$

Therefore, the equation for track error can be expressed as:

$$\begin{cases} e_{a1} = x_{a1} - z_{a1} \\ \dot{e}_{a1} = e_{a2} - \beta_1 e_{a1} \\ \dot{e}_{a2} = e_{a3} - \beta_2 e_{a2} + ce_1 \\ \dot{e}_{a3} = -\beta_3 e_{a3} - p(t) \end{cases} \quad (25)$$

where it is noted that  $c = \frac{4k_{as}}{m}$  and  $e_{a2}, e_{a3}$  can be rewritten as:

$$e_{a2} = \dot{e}_{a1} + \beta_1 e_{a1} \quad (26)$$

$$e_{a3} = \ddot{e}_{a1} + \beta_1 \dot{e}_{a1} + \beta_2 (\dot{e}_{a1} + \beta_1 e_{a1}) - ce_1 \quad (27)$$

The verifications for stability and amelioration of error convergence are presented as follows:

Define  $\mathbf{Y} = [y_1 y_2 y_3]$ ,  $y_1 = e_{a1}, y_2 = e_{a2} - \beta_1 e_{a1}, y_3 = e_{a3} - (\beta_1 + \beta_2) e_{a2} + (\beta_1^2 + c) e_{a1}$ , and (25) is rewritten as:

$$\begin{cases} \dot{y}_1 = y_2 \\ \dot{y}_2 = y_3 \\ \dot{y}_3 = -k_1 y_1 - k_2 y_2 - k_3 y_3 - p(t) \end{cases} \quad (28)$$

where  $k_1 = \beta_1 \beta_2 \beta_3 - c \beta_3, k_2 = \beta_1 \beta_2 + \beta_2 \beta_3 + \beta_1 \beta_3 - c, k_3 = \beta_1 + \beta_2 + \beta_3$ , and the characteristic equation of (28) is expressed as:

$$f(\lambda) = \lambda^3 + k_3 \lambda^2 + k_2 \lambda + k_1 \quad (29)$$

As long as the roots of (30) have negative real parts, the stability and convergence of  $\mathbf{Y}$  will be guaranteed. According to Routh-Hurwitz conditions, the parameters to be met are as follows:

$$\begin{cases} k_3 = \beta_1 + \beta_2 + \beta_3 > 0 \\ k_1 = \beta_1 \beta_2 \beta_3 - c \beta_3 > 0 \\ k_3 k_2 - k_1 = (\beta_1 + \beta_2)(\beta_1 \beta_3 + \beta_2 \beta_3 + \beta_3^2 + \beta_1 \beta_2 - c) > 0 \end{cases} \quad (30)$$

(30) assures that track errors  $\mathbf{e}$  are bounded and convergent. Since  $|p(t)| \leq p_0$ , when the system reaches a steady state, it is noted that

$$\begin{cases} \dot{y}_1 = y_2 = 0 \\ \dot{y}_2 = y_3 = 0 \\ \dot{y}_3 = 0 \end{cases} \quad (31)$$

Finally, the boundary of track errors  $\mathbf{e}$  can be given as:

$$\begin{cases} \|e_{a1}\|_\infty = \frac{1}{\beta_1 \beta_2 \beta_3 - c \beta_3} p_0 \\ \|e_{a2}\|_\infty = \frac{\beta_1}{\beta_1 \beta_2 \beta_3 - c \beta_3} p_0 \\ \|e_{a3}\|_\infty = \frac{1}{\beta_3} p_0 \end{cases} \quad (32)$$

In contrast to the boundary of track errors  $\mathbf{e}$  with the improved linear extended state observer, the boundary of track errors  $\mathbf{e}'$  with the traditional LESO applied in the MISP control system can be obtained (with identical gain) and expressed as:

$$\begin{cases} \|e'_{a1}\|_\infty = \frac{1}{\beta_3} p_0 \\ \|e'_{a2}\|_\infty = \frac{\beta_1}{\beta_3} p_0 \\ \|e'_{a3}\|_\infty = \frac{\beta_2 - c}{\beta_3} p_0 \end{cases} \quad (33)$$

Comparing the results in (32) and (33), the observed accuracy with the improved LESO is greatly improved under the condition that  $|\beta_1 \beta_2 - c| > 1$  and  $|\beta_2 - c| > 1$ . Generally, the convergence speed of the proposed method is controlled by adjusting gain parameters based on the stability of the system. Nevertheless, in practical engineering applications, high gain will result in a deterioration of dynamic performance. With the same error accuracy, the improved LESO can adopt a smaller gain than the traditional LESO.

### C. VIBRATION ISOLATION CONTROLLER

The controller designed for the active vibration isolation controller  $G_{ia}(s)$  meets the following requirements:

- 1) The estimated input vibration force  $\hat{f}_z$  can compensate for the effect of the real input  $f_z$  with  $G_{ia}(s)$ .
- 2)  $G_{ia}(s)$  is independent of the original control channel for levitation.

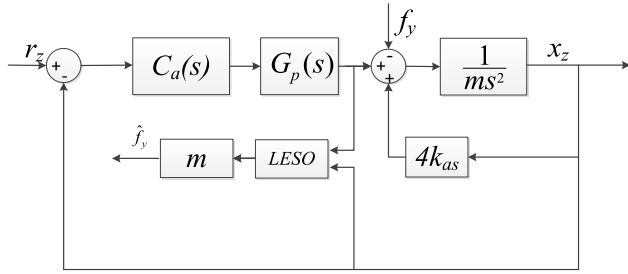


FIGURE 6. Axial displacement control system with complete active isolation control.

Therefore, controller  $G_{ia}(s)$  should be designed as follows:

$$G_{ia}(s) = \frac{1}{C_\alpha(s)G_p(s)} \quad (34)$$

The control system with  $G_{ia}(s)$  is presented in Fig. 6.

As depicted in Fig. 6, the improved LESO and the controller  $G_{ia}(s)$  make up the channel of active vibration control, and the input vibration force  $f_z$  is compensated and offset under the series connection with the suspension control channel.

By substituting (16) and (17) into controller (34),  $G_{ia}(s)$  is rewritten as:

$$G_{ia}(s) = (\tau_f s + 1)(\tau_{mag} s + 1) \times \frac{(0.0001s + 1)s}{(k_d + 0.0001k_p)s^2 + (k_p + 0.0001k_i)s + k_i} \quad (35)$$

Actually,  $(\tau_f s + 1)$  and  $(\tau_{mag} s + 1)$  are physically inaccessible and are replaced by  $(\frac{\tau_f s}{0.0001s + 1} + 1)$  and  $(\frac{\tau_{mag} s}{0.0001s + 1} + 1)$ . Eventually, the controller  $G_{ia}(s)$  is designated as follows:

$$G_{ia}(s) = \left(\frac{\tau_f s}{0.0001s + 1} + 1\right) \left(\frac{\tau_{mag} s}{0.0001s + 1} + 1\right) \times \frac{(0.0001s + 1)s}{(k_d + 0.0001k_p)s^2 + (k_p + 0.0001k_i)s + k_i} \quad (36)$$

IV. SIMULATION AND ANALYSIS

To confirm the validity of the proposed method, a simulation is conducted as follows. As the relative experiment is still under research, only the simulation result is presented in this paper. The relative parameters are provided in Table 1.

In Fig. 7, the thick dotted line depicts the frequency response result without the LESO or active isolation controller, which has already been illustrated in Fig. 5. The dashed line and the centerline depict the frequency response results of employing the active isolation system combined with the original LESO and improved LESO, respectively.

As Fig. 7 shows, compared with the initial system without any measures, the magnitude of the frequency response declines obviously when active vibration isolation control is adopted in the MISP system. We can see that the magnitude falls to approximately -60 dB at 1 Hz but rises to over 0 dB as the frequency increases when the active isolation controller and original LESO are applied in the control system. This implies that the isolation effect will worsen with increasing

TABLE 1. System parameters of MISP and control system.

Parameter	Symbol	Value	Unit
Mass	$m$	124	kg
Radial moment of inertia	$J_r$	1.638	kg/m <sup>2</sup>
Displacement stiffness	$k_{as}$	2192	N/mm
Time constant of power amplifier	$\tau_{mag}$	0.0005	s
Proportional coefficient	$K_p$	15000	/
Differential coefficient	$K_d$	60	/
Integral coefficient	$K_I$	150000	/
Time constant of filter	$\tau_f$	0.00128	/
Gain of improved LESO	$\beta_1$	10	/
	$\beta_2$	100	/
	$\beta_3$	1000	/

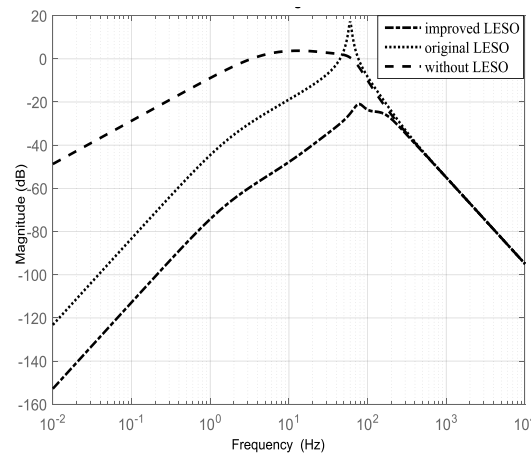
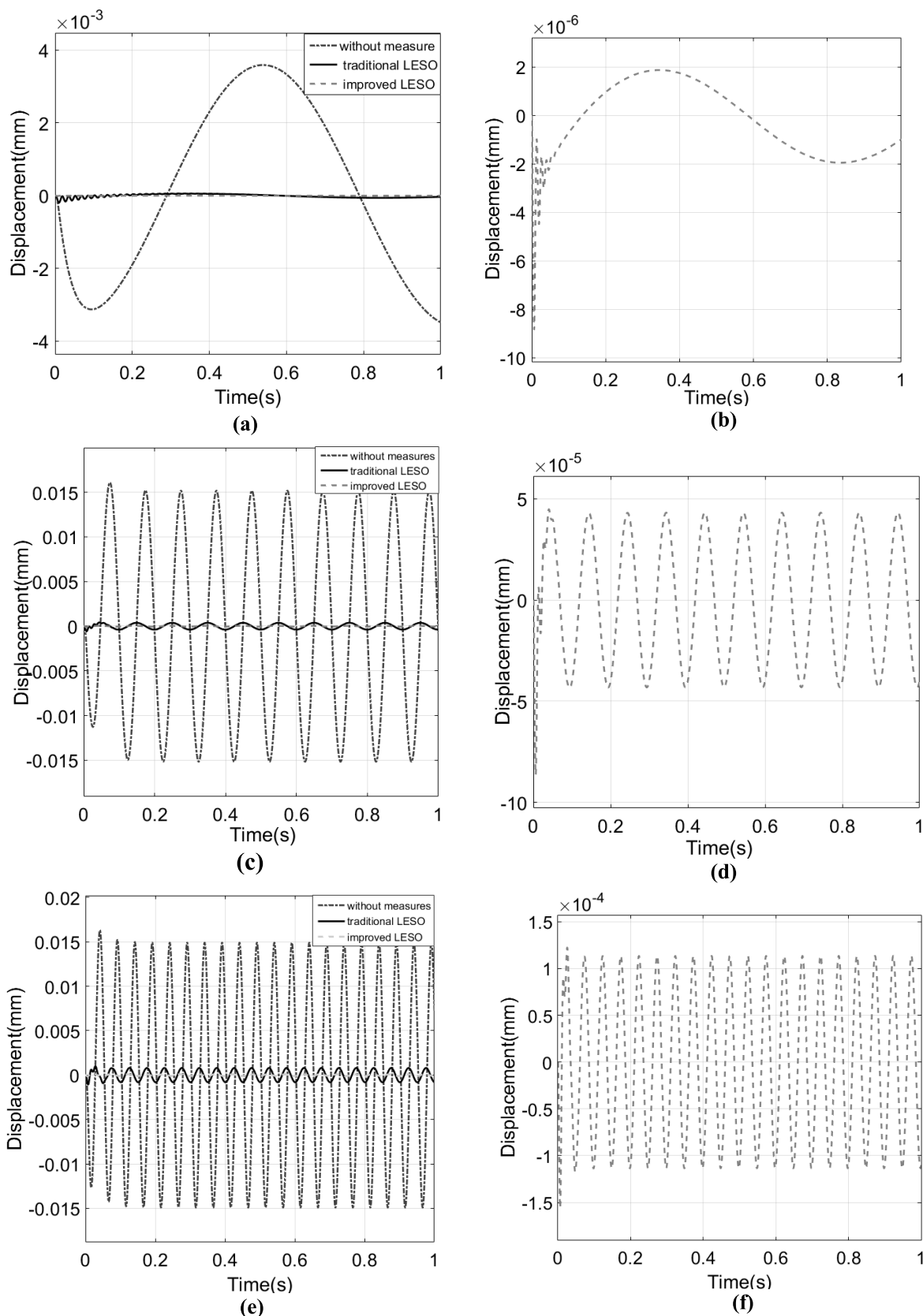


FIGURE 7. Frequency response of the input vibration transfer function based on linear analysis.

input vibration frequency and that there is no notable isolation effect with the original LESO. For the system with the improved LESO and active isolation controller, the magnitude in the entire required frequency band (1-20 Hz) is apparently lower than the former when the input vibration frequency increases. The frequency response results indicate that vibration suppression is ameliorated with the combination of an improved LESO and an active vibration isolation controller.

To validate the above analysis, we simulate input vibration signals of different frequencies that are represented by sine functions as  $y_{z1} = 0.01 \sin(2\pi t)$ ,  $y_{z2} = 0.01 \sin(2\pi \times 10t)$ ,  $y_{z3} = 0.01 \sin(2\pi \times 20t)$ . This means that the amplitude of the input vibration displacement from the base is 0.01 millimeters, and the frequencies are 1 Hz,



**FIGURE 8.** Axial displacement output at different input vibration frequencies: (a) Simulation results of 1 Hz input vibration signal (b) Enlarged view of at 1 Hz with improved LESO (c) Simulation results of 10 Hz input vibration signal (d) Enlarged view at 10 Hz with improved LESO (e) Simulation results of 20 Hz input vibration signal (f) Enlarged view at 20 Hz with improved LESO.

10 Hz, and 20 Hz. The results of the output  $x_z$  are shown in Fig. 8, and the data are presented in Table 2.

As shown in the simulation results, the effectiveness of active vibration isolation control is verified, and the improved

TABLE 2. Simulation results.

Input frequency (Hz)	Output without measures (mm)	Output with traditional LESO (mm)	Output with improved LESO (mm)
1	$3.6 \times 10^{-3}$	$1.9 \times 10^{-5}$	$1.9 \times 10^{-6}$
10	$1.5 \times 10^{-2}$	$3.8 \times 10^{-4}$	$4.3 \times 10^{-5}$
20	$1.5 \times 10^{-2}$	$8 \times 10^{-4}$	$1.2 \times 10^{-4}$

LESO adopted in the MISP control system ameliorates the vibration isolation effect at low frequencies compared with the traditional LESO. Generally, although the vibration isolation performance will degrade as the frequency of vibration increases, the improved LESO still has significant advantages in vibration isolation accuracy at different frequencies. Under vibration inputs of 1 Hz, 10 Hz and 20 Hz, the displacement output was reduced by 90%, 88.7%, and 85%, respectively, compared with that of the traditional LESO.

## V. CONCLUSION

This paper studies a low-frequency vibration isolation technique for a MISP. Concerning the limitation of mechanical vibration isolation, an improved linear extended state observer is designed, and active vibration isolation compensation control is put forward. As confirmed by simulation results, the proposed method has several implications. First, the estimation accuracy of low-frequency input vibration on a MISP is enhanced with an improved LESO to provide an effective data basis for subsequent vibration compensation. Second, the design and introduction of an active vibration isolation controller compensates for the input vibration. Finally, the combination of the LESO and active vibration isolation controller is effective in eliminating negative effects from low-frequency input vibrations, which is difficult to achieve by mechanical measures. In further studies, more attention will be paid to the optimization of the model structure and control system, such as considering model uncertainty and additional research on dual-stage control, which is a control method coordinating the work of the framework and platform. The improvement of the control system will be robust against all kinds of disturbances.

## REFERENCES

- [1] W. W. Anderson, N. J. Groom, and C. T. Woolley, "Annular suspension and pointing system," *IFAC Proc. Volumes*, vol. 12, no. 4, pp. 41–49, 1979.
- [2] D. C. Cunningham, T. P. Gismondi, and G. W. Wilson, "Control system design of the annular suspension and pointing system," *J. Guid. Control*, vol. 3, no. 1, p. 11 21, 1980.
- [3] L. Zhuchong, L. Kun, and Z. Wei, "Inertially stabilized platform for airborne remote sensing using magnetic bearings," *IEEE/ASME Trans. Mechatronics*, vol. 21, no. 1, pp. 288–301, Feb. 2016.
- [4] J. Fang, C. Wang, and T. Wen, "Design and optimization of a radial hybrid magnetic bearing with separate poles for magnetically suspended inertially stabilized platform," *IEEE Trans. Magn.*, vol. 50, no. 5, pp. 1–11, May 2014.
- [5] J. Mao, S. Li, Q. Li, and J. Yang, "Design and implementation of continuous finite-time sliding mode control for 2-DOF inertially stabilized platform subject to multiple disturbances," *ISA Trans.*, vol. 84, pp. 214–224, Jan. 2019.
- [6] D. Wang and H. Sun, "Design of repetitive controller based on linear auto disturbance rejection control for active magnetic bearing spindles," in *Proc. 2nd Int. Conf. Cybern., Robot. Control (CRC)*, Jul. 2017, pp. 106–110.
- [7] H.-P. Lee and I.-E. Yoo, "Robust control design for a two-axis gimbaled stabilization system," in *Proc. IEEE Aerosp. Conf.*, Mar. 2008, pp. 1–7.
- [8] J. M. Hilkert, "Inertially stabilized platform technology concepts and principles," *IEEE Control Syst. Mag.*, vol. 28, no. 1, pp. 26–47, Feb. 2008.
- [9] J. M. Hilkert and B. Pautler, "A reduced-order disturbance observer applied to inertially stabilized line-of-sight control," in *Proc. SPIE, Acquisition, Tracking, Pointing, Laser Syst. Technol. XXV*, vol. 8052, May 2011, Art. no. 80520H, doi: [10.1117/12.884123](https://doi.org/10.1117/12.884123).
- [10] J. A. R. K. Moorthy, "Fuzzy controller for line-of-sight stabilization systems," *Opt. Eng.*, vol. 43, no. 6, pp. 1394–1401, 2004.
- [11] D. L. Trumper, S. M. Olson, and P. K. Subrahmanyam, "Linearizing control of magnetic suspension systems," *IEEE Trans. Control Syst. Technol.*, vol. 5, no. 4, pp. 427–438, Jul. 1997.
- [12] P. Tsiotras and B. C. Wilson, "Zero- and low-bias control designs for active magnetic bearings," *IEEE Trans. Control Syst. Technol.*, vol. 11, no. 6, pp. 889–904, Nov. 2003.
- [13] A. Javadi and S. Pezeshki, "A new model-free adaptive controller versus non-linear  $H_\infty$  controller for levitation of an electromagnetic system," *Trans. Inst. Meas. Control*, vol. 35, no. 3, pp. 321–329, May 2013.
- [14] P. S. V. Nataraj and M. D. Patil, "Robust control design for nonlinear magnetic levitation system using quantitative feedback theory (QFT)," in *Proc. Annu. IEEE India Conf.*, Dec. 2008, pp. 365–370.
- [15] K. Cai, C. Peng, Z. Deng, and K. Li, "Vibration suppression control for MSFW with gyroscopic effects using synchronous rotate frame," in *Proc. 37th Chin. Control Conf. (CCC)*, Jul. 2018, pp. 3756–3760.
- [16] W. Zhang and T. Wang, "Research on magnetic suspended vibration isolation system based on stiffness control under base motion," in *Proc. Chin. Control Decis. Conf. (CCDC)*, Jun. 2018, pp. 5314–5318.
- [17] X. Sun and A. Baz, "Active vibration isolation platform based on a vector algorithm," in *Proc. WRI World Congr. Comput. Sci. Inf. Eng.*, Mar. 2009, pp. 97–101.
- [18] M. Zhai, X. Li, and S. Liu, "Research on the design of mechanical and electromagnetic composite vibration isolation system," in *Proc. Prognostics Syst. Health Manage. Conf. (PHM-Hunan)*, Aug. 2014, pp. 553–558.
- [19] W. Fu, Z. Qian, X. Huang, and F. Tan, "Analysis of two-stage passive vibration isolation system for crystal oscillator at high-frequency vibration," in *Proc. IEEE Int. Freq. Control Symp. Joint with 22nd Eur. Freq. Time forum*, Apr. 2009, pp. 501–504, doi: [10.1109/FREQ.2009.5168230](https://doi.org/10.1109/FREQ.2009.5168230).
- [20] Y. Hu, C. Chen, H. Wu, and C. Song, "Study on structural optimization design and cascade PID control of maglev actuator for active vibration isolation system," *J. Vib. Control*, vol. 24, no. 10, pp. 1829–1847, Jun. 2018.
- [21] G. Wang, M. Chadli, and M. Basin, "Practical terminal sliding mode control of nonlinear uncertain active suspension systems with adaptive disturbance observer," *IEEE/ASME Trans. Mechatronics*, early access, Jun. 5, 2020, doi: [10.1109/TMECH.2020.3000122](https://doi.org/10.1109/TMECH.2020.3000122).
- [22] Y. Yanyu, F. Zhihao, W. Yong, and J. Ping, "Extended disturbance observer based robust control for vibration isolation on airborne optoelectronic platform," in *Proc. 34th Chin. Control Conf. (CCC)*, Jul. 2015, pp. 4343–4348, doi: [10.1109/ChiCC.2015.7260312](https://doi.org/10.1109/ChiCC.2015.7260312).
- [23] T. Yang, N. Sun, H. Chen, and Y. Fang, "Observer-based nonlinear control for tower cranes suffering from uncertain friction and actuator constraints with experimental verification," *IEEE Trans. Ind. Electron.*, early access, May 12, 2020, doi: [10.1109/TIE.2020.2992972](https://doi.org/10.1109/TIE.2020.2992972).
- [24] Z. Lin, K. Liu, L. Zhang, and D. Zeng, "Coupling effect and control strategies of the maglev dual-stage inertially stabilization system based on frequency-domain analysis," *ISA Trans.*, vol. 64, pp. 98–112, Sep. 2016.
- [25] J. Sun, C. Wang, and R. Xin, "On disturbance rejection control of servo system based on the improved disturbance observer," in *Proc. 37th Chin. Control Conf. (CCC)*, Jul. 2018, pp. 2554–2559.
- [26] Z. Gao, "Scaling and bandwidth-parameterization based controller tuning," in *Proc. Amer. Control Conf.*, 2003, pp. 4989–4996.
- [27] J. Han, "A class of extended state observers for uncertain systems," (in Chinese), *Control Decis.*, vol. 10, no. 1, pp. 85–88, 1995.
- [28] D. Sun and Y. Zhang, "Improvement and observation accuracy analysis of linear extended state observer," (in Chinese), *J. Nat. Univ. Defense Technol.*, vol. 39, no. 6, pp. 111–117, 2017.





**WANFA SHI** was born in Guangdong, China, in 1993. He received the B.S. and M.S. degrees in mechanical and electronics engineering for Central South University, Changsha, China, in 2015 and 2018, respectively. He is currently pursuing the Ph.D. degree in engineering mechanics with Sun Yat-sen University, Guangzhou, China. His current research interests include design, dynamics, and control of magnetic suspension systems and inertially stabilized platform.



**WENPENG ZHAO** (Member, IEEE) received the B.Eng. degree in electrical engineering from Tongji University, Shanghai, China, in 2018. He is currently pursuing the M.S. degree in mechatronics with Sun Yat-Sen University, Guangzhou, Guangdong, China. His current research interest includes motor control system design.

...



**KUN LIU** received the B.Eng. and M.Eng. degrees from the Beijing University of Aeronautics and Astronautics, Beijing, China, in 1985 and 1988, respectively, and the Ph.D. degree in hybrid rocket motor from the National University of Defense Technology, Changsha, China, in 1999. He is currently a Professor and a Ph.D. Candidate Supervisor with the College of Aerospace Science and Engineering, Sun Yat-sen University. His teaching covers attitude dynamics and control of spacecraft and linear system. His research interests include design, dynamics, and control of magnetic suspended flywheel and control moment gyroscope, and dynamics and control of spacecraft.